AASERT Grant #N00014-93-1-0827

Fourth Semi-Annual Progress Report
(covering the period of 02/15/95-07/25/95)

Project Title: Investigation of Normal Incidence High-Performance P-type Strained Layer InGaAs/AlGaAs and GaAs/AlGaAs Quantum Well Infrared Photodetectors.

Submitted to

Max N. Yoder

Office of Naval Research
Code 3140
800 North Quincy Street
Arlington, VA   22217-5000
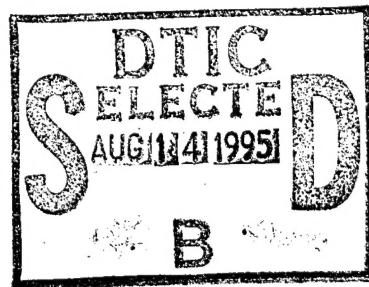
Prepared by

Jerome T. Chu   and   Sheng S. Li
Student   Professor

Department of Electrical Engineering
University of Florida
Gainesville, FL   32611

Tel. (904) 392-4937
Fax (904) 392-8671
E-mail: ShengLi@ENG.UFL.EDU

July 31, 1995

DTIC QUALITY INSPECTED 5

19950810 025

REPORT DOCUMENTATION PAGE

1. AGENCY USE ONLY (Leave blank)	2. REPORT DATE 31 July 1995	3. REPORT TYPE AND DATES COVERED Progress Report: 02/16/95-07/25/95

4. TITLE AND SUBTITLE
Investigation of Normal Incident High Performance P-type Strained Layer InGaAs/AlGaAs and GaAs/AlGaAs QWIPs

5. FUNDING NUMBERS
ONR #N00014-93-1-0827

6. AUTHOR(S)
Jerome T. Chu, Student
Sheng S. Li, Professor

7. PERFORMING ORGANIZATION NAME(S) AND ADDRESS(ES)
University of Florida
Gainesville, FL 32611-6200

8. PERFORMING ORGANIZATION REPORT NUMBER
92120712

9. SPONSORING/MONITORING AGENCY NAME(S) AND ADDRESS(ES)
US Navy, Office of Naval Research
800 North Quincy Street, Code 1512B:SM
Arlington, VA 22217-5000

10. SPONSORING/MONITORING AGENCY REPORT NUMBER

11. SUPPLEMENTARY NOTES

12a. DISTRIBUTION/AVAILABILITY STATEMENT
Approved for public release, distribution unlimited.

12b. DISTRIBUTION CODE

13. ABSTRACT (Maximum 200 words)

During this reporting period, we have made excellent progress towards the program goals. A significant achievement was made in the development of a new compressively strained p-type InGaAs/AlGaAs QWIP grown on GaAs by MBE with very low dark current densities. This new QWIP achieved two color detection with detection peaks at 7.4 μm in the LWIR band and 5.5 μm in the MWIR band. This detector is under background limited performance (BLIP) at temperatures up to 67 K, with operation possible at temperatures greater than 85 K. The measured responsivity was found to be 40 mA/W for the LWIR peak, while a responsivity of 8 mA/W was found for the MWIR peak; all at T=77 K. In addition, the measured detectivity was found to be 1.06×10^{10} Jones at T=81 K and 1.0 V of applied bias. In addition, two new compressively strained p-QWIPs with detection peaks at 9.2 μm and 10.1 μm were characterized. Responsivities of 28 mA/W at T=45 K and V=-2.5 V and 17 mA/W at T=55 K and -1.0 V were measured at the 9.2 μm and 10.1 μm peaks respectively. The 9.2 μm p-QWIP has an estimated D* of 2.7×10^9 Jones, while the 10.1 μm peak p-QWIP has an estimated D* of 1.04×10^9 Jones. Finally, a Si-doped unstrained p-QWIP grown on (311) Si GaAs was characterized. This p-QWIP exhibits extremely symmetrical dark current characteristics and has two MWIR detective peaks at 3.0 μm and 5.2 μm.

14. SUBJECT TERMS
P-type strained layer InGaAs/GaAs quantum well infrared photodetectors (QWIPs), intersubband absorption, dark current, responsivity, detectivity.

15. NUMBER OF PAGES

16. PRICE CODE

17. SECURITY CLASSIFICATION OF REPORT	18. SECURITY CLASSIFICATION OF THIS PAGE	19. SECURITY CLASSIFICATION OF ABSTRACT	20. LIMITATION OF ABSTRACT
Unclassified			Unlimited

Fourth Semi-Annual Progress Report (2/1/95-7/25/95)

Project Title: The Development of Normal Incidence High Performance
P-type Strained Layer InGaAs/AlGaAs Quantum Well
Infrared Photodetectors

Program Manager: Max N. Yoder, Office of Naval Research, Code 3140, Arlington, VA.

Principal Investigator: Sheng S. Li, Professor, University of Florida, Gainesville, FL.

Student : Jerome T. Chu

Project Objective:

The objective of this project is to perform theoretical and experimental studies of dark current, photocurrent, optical absorption, spectral responsivity, noise, and detectivity for the normal incidence strained layer p-type III-V semiconductor quantum well infrared photodetectors (QWIPs) developed under this program. The material systems under investigation include InGaAs/InAlAs on InP substrates and GaAs/InGaAs or AlGaAs/InGaAs on GaAs substrates. The project will study the usage and effects of biaxial tension and compressional strain on the material systems and their effects towards photodetector design.

- 1 -

I. Introduction

During the period of February 1, 1995 to July 25, 1995, significant progress has been made towards the design, fabrication, and characterization of new strained layer p-type GaAs/InGaAs on GaAs and InGaAs/AlGaAs on GaAs quantum-well infrared photodetectors (P-QWIPs) in the 8-14 μm range for staring focal plane arrays (FPAs). Specific tasks performed during this period include: (i) the continuing characterization of a normal incidence strained-layer p-type AlGaAs/InGaAs QWIP grown on a GaAs substrate with a peak long wavelength infrared (LWIR) detective wavelength at 7.4 μm and a mid-wavelength infrared (MWIR) detection peak at 5.5 μm, with extremely low dark currents, by utilizing a thinned substrate waveguide-like structure to improve responsivity, (ii) the characterization of a novel Si-doped p-QWIP on a semi-insulating (SI) (311) GaAs substrate with MWIR detective peaks at 3.0 and 5.2 μm, and highly symmetric dark current characteristics, and (iii) the characterization of two new Be-doped strained-layer p-QWIPs based upon the previously mentioned two-color two-band AlGaAs/InGaAs QWIP, with detection peaks at 9.3 μm and 10.1 μm, and with reasonable dark current densities. The following sections of this report will cover the technical results of the study obtained during this reporting period and the research accomplishments and publications. A summary of the complete study is listed at the end of this report in table 1.

II. Technical Results

2.1 Research Accomplishments and Publications

1. The design, growth, fabrication, and characterization of a strained InGaAs/AlGaAs P-QWIP on a GaAs substrate with a peak wavelength of 7.5 μm and a mid-wavelength infrared (MWIR) peak at 5.5 μm. Very low dark current densities for this device were measured at 77 K. Maximum responsivities of 40 mA/W and 8 mA/W were measured for each respective wavelength at 77 K under an applied bias of +5.0 V with operation at up to 85 K possible under moderate bias ($\leq$ 2 V). BLIP condition was achieved in both detection bands at 63 K within the applied bias range of -2.7 V to 3.0 V. Measured detectivity at T = 81 K and V = 1.0 V was 1.06×10^{10} cm$\sqrt{Hz}$/W. By

improving the responsivity of this p-QWIP by means of changing the physical structure of the detector and not the quantum well layers, we were able to achieve an increase in detectivity to about 1.66×10^{10} cm$\sqrt{Hz}$/W, under the previous conditions. In addition, extensive noise characterization studies were performed and the results are presented.

2. The design, growth, fabrication, and characterization of a Si-doped InGaAs/AlGaAs p-QWIP on a (311) GaAs substrate with peak wavelength at 3.0 and 5.2 μm in the MWIR band. Highly symmetrical dark current densities were found for this unstrained device at all measured temperatures (40 K to 120 K).

3. The design, growth, fabrication, and characterization of two Be-doped compressively strained InGaAs/AlGaAs p-QWIPs on SI GaAs substrates with peak wavelengths at 9.3 and 10.1 μm, respectively. The 9.3 μm p-QWIP exhibits a peak responsivity of 28 mA/W at T = 45 K under a bias of -2.5 V; while the 10.1 μm p-QWIP exhibits a maximum responsivity of 17 mA/W at a temperature of T = 55 K and at an applied bias of -1.0 V. BLIP condition for the 9.2 μm p-QWIP can be achieved for positive biases under 2.0 V and at temperatures less than 45 K. Similarly, the 10.1 μm p-QWIP exhibits BLIP conditions when the applied bias is under 1.0 V at T = 46 K.

A. Journal Papers:

1. Y. H. Wang, S. S. Li, and J. Chu and Pin Ho, "An Ultra-low Dark Current P-type Strained-layer InGaAs/InAlAs Quantum Well Infrared Photodetector with Background Limited Performance (BLIP)" *Appl. Phys. Letts*, **64**(4), 727 (1994).

2. Y. H. Wang, S. S. Li, and J. Chu and Pin Ho, "A Normal Incidence P-type Compressive Strained-Layer InGaAs/GaAs Quantum Well Infrared Photodetector for Mid-Wavelength Infrared (MWIR) and Long-Wacelength Infrared (LWIR) Detection" *J. Appl. Phys.*, **76**(10), 6009 (1994).

3. D. C. Wang, G. Bosman, and S. S. Li, "Noise Characterization and Device Parameter Extraction on a p-type Strained Layer Quantum Well Infrared Photodetector", submitted to *J. Appl. Phys.*, July 18, 1995.

B. Conference Presentations:

1. S. S. Li, J. Chu, and Y. H. Wang, "A Normal Incidence P-type Strained Layer In-GaAs/InAlAs Quantum Well Infrared Photodetector with Background Limited Performance at 77 K", presented at the 1994 SPIE symposium, Orlando, FL, April 4-8, 1994. Full paper published in the conference proceedings.

2. Pin Ho, Y. H. Wang, S. S. Li, and J. Chu, "MBE Growth of P-type Strained-layer InGaAs/InAlAs QWIPs", presented at the 1994 14th North American Conference on Molecular-beam Epitaxy, Urbana-Champaign, IL, October 10-12, 1994.

3. Y. H. Wang, J. Chu, S. S. Li, and Pin Ho, "A Normal Incidence P-type Compressive Strained-Layer InGaAs/GaAs Quantum Well Infrared Photodetector", 2nd. International Conference on 2-20 μm Wavelength Infrared Detectors and Arrays, Miami Beach, FL, October 9-14, 1994. Full paper published in the conference proceedings.

4. S. S. Li, Y. H. Wang, and J. Chu, "A New Class of Normal Incidence Strained-Layer III-V Quantum Well Infrared Photodetectors", presented at the 1994 LEOS Conference, Boston, MA, October 31-November 3, 1994.

5. J. Chu, Y. H. Wang, S. S. Li, and Pin Ho, "A New Compressively Strained In-GaAs/AlGaAs p-type Quantum Well Infrared Photodetector with Ultra-low Dark Current and Detective Peaks in the LWIR and MWIR Bands", accepted for presentation at the 3rd. International Symposium on Long Wavelength Infrared Detectors and Arrays: Physics and Applications, Chicago, IL, October 9-11, 1995. Full paper to be published in the conference proceedings.

6. J. Chu, S. S. Li, S. Y. Yen, A. Chin, and K. M. Chang, "Investigation of Si-doped p-type GaAs/AlGaAs and Strained-layer InGaAs/AlGaAs Quantum Well Infrared Photodetectors grown on (311) GaAs for Mid- and Long-Wavelength IR Detection", accepted for presentation at the 3rd. International Symposium on Long Wavelength Infrared Detectors and Arrays: Physics and Applications, Chicago, IL, October 9-11, 1995.

7. D. Wang, G. Bosman, S. S. Li, and J. Chu, "Noise Performance of p-type Strained Layer Quantum Well Infrared Photodetectors", accepted for presentation at the 3rd.

International Symposium on Long Wavelength Infrared Detectors and Arrays: Physics and Applications, Chicago, IL, October 9-11, 1995.

2.2 P-QWIP Operation and Design Theory

With the advent of advanced molecular beam expitaxial technologies in the last few decades, device structures utilizing heterostructure quantum wells have been heavily explored. N-type quantum well infrared photodetectors (QWIPs) have been extensively studied in recent years[1-2,28]. These systems use GaAs/AlGaAs and InGaAs/InAlAs structures for detection in the 3 - 5 μm mid-wavelength infrared (MWIR) and 8 - 14 μm LWIR atmospheric transmission windows. Since n-type GaAs/InGaAs and InGaAs/InAlAs QWIPs have inherently low electron effective masses and high electron mobilities, they offer excellent infrared (IR) detection properties. Due to the quantum mechanical selection rules which prohibit normal incidence intersubband absorption, focal plane arrays (FPA) using n-type QWIPs must use either metal or dielectric gratings to couple normal incidence IR radiation into the quantum well[2-4]. In contrast, because of the mixing between the light hole and heavy hole states under either biaxial tension or compressive strain, normal incidence illumination is allowed for the intersubband transition in p-type QWIPs; thus eliminating the need for metal or dielectric grating couplers.

2.2.1 P-QWIP Physics

2.2.1.1 Strained Layer Growth Limitations and Theory

P-type QWIPs using valence intersubband transitions have been demonstrated[5-7] in lattice-matched GaAs/AlGaAs and InGaAs/InAlAs material systems. In general, intersubband transitions excited by normal incidence radiation in p-type quantum wells are allowed since a linear combination of p-like valence band Bloch states exists, which provides a nonzero coupling between the normal radiation field and valence band Bloch states. The strong mixing between the heavy hole and the light hole states greatly enhances intersubband absorption. The drawback of using lattice-matched systems is the fact that the intersubband transition occurs between the heavy hole ground states and the upper excited states. Because of the relatively large heavy hole effective mass when compared to the electron effective

mass, relatively weak absorption and therefore similarly low responsivity is predicted in the IR wavelength range when compared to n-type QWIPs. In order to increase the absorption characterisitics and responsivity of P-QWIPs, biaxial stress is introduced into the well layers of the QWIP structure. If the intentionally introduced biaxial stress between the well layers and the barrier layers contained in the layer thickness (the total thickness of the wells and barriers) in the P-QWIP structure is less than the critical thickness, then pseudomorphic or coherent heterointerfaces can be grown without the introduction of defects between the layers. Based upon the force balance model[8,29-30], the equilibrium critical layer thickness, L_c, for an epilayer with the lattice constant, a, grown on a substrate with a lattice constant, a_s, is given as

$$L_c = \left(\frac{a}{\sqrt{2}\delta_o}\right) \frac{1 - \nu \cos^2 \Theta}{8\pi(1 + \nu)\cos\alpha} \left[1 + \ln(h\sqrt{2}/a)\right], \tag{1}$$

where h is the epilayer thickness, Θ is the angle between the dislocation line and the Burges' vector, α is the angle between the slip direction and the layer plane direction, δ_o is the lattice-mismatch or the in-plane strain, and ν is the Poisson ratio. δ_o is defined as $\delta_o = (a_s - a)/a$ where $\delta_o > 0$ for tensile strain and $\delta_o < 0$ for compressive strain. Similarly, ν is defined as $\nu = -C_{12}/C_{11}$. C_{ij}'s are the elastic constants and can be found in reference 9.

The strained-layers have the same effective in-plane lattice constant, $a_\parallel$ (i.e., $a_{x,y}$), and can store the excess energy due to the elastic strain within the layers. The in-plane lattice constant, $a_\parallel$, can be expressed by[8]

$$a_\parallel = a_1 \left[1 + \delta_o/\left(1 + \frac{\xi_1 L_1}{\xi_2 L_2}\right)\right], \tag{2}$$

where $a_{1,2}$ and $L_{1,2}$ are the individual layer lattice constants and thicknesses, respectively, and $\xi_{1,2}$ are the shear moduli as described by $\xi = (C_{11} + C_{12} - 2C_{12}^2/C_{11})$, where the C_{ij}'s are elastic constants for the strained material. δ_o denotes the lattice mismatch between layers and $a_{1,2}$ are the lattice constants of the strained well and the substrate (or barrier) respectively. When $a_\parallel \neq a_s$, the coherently strained superlattice structure is no longer in equilibrium with the substrate. If the lattice constant of the barrier layers is equal to that of the substrate, the the strain will be completely accomodated in the well layers with no strain in the barrier layers. However, Hull et al.[22] showed that if the individual layer thickness in the superlattice is less than its critical thickness, even though $a_\parallel \neq a_s$, the loss of coherence only occurs at the interface between the whole superlattice and the substrate, while the

superlattice itself remains coherent.

2.2.1.2 Strain Induced Energy Band Shifts

If the QWIP structure is grown along the [100] direction and the strained-layer is within the critical thickness, L_c, then a pseudomorphic or coherent heterointerface can be obtained and the components of the strain tensor [e] are simplified to the expressions given by

$$e_{xx} = e_{yy} = e_{\parallel} \tag{3}$$

$$e_{zz} = -e_{\parallel}\left(\frac{2C_{12}}{C_{11}}\right) \tag{4}$$

$$e_{xy} = e_{yz} = e_{zx} = 0. \tag{5}$$

In addition to altering the physical parameters of the QWIP, lattice strain can also induce energy band shifts, which can be used to alter the absorption characteristics of the QWIP. The strain induced energy band shifts for the conduction band, the heavy hole subband, and light hole subband can be approximated as follows.

$$\Delta E_c = 2c_1\frac{C_{11} - C_{12}}{C_{11}}\delta_o \tag{6}$$

$$\Delta E_{hh} = b\frac{C_{11} + C_{12}}{C_{11}}\delta_o \tag{7}$$

$$\Delta E_{lh} = -\Delta E_{hh} + \frac{(\Delta E_{hh})^2}{2\Delta_o} \tag{8}$$

where c_1 is the combined hydrostatic deformation potential which characterizes the splitting of the Γ_8 valence band under strain, and b is the shear deformation potential, and Δ_o is the spin orbit split-off energy[9]. The total hydrostatic deformation potential $(c_1 + V_v)$, where V_v is the valence band deformation potential, can be expressed by[10]

$$c_1 + V_v = -\frac{1}{3}(C_{11} + 2C_{12})\frac{dE_g^o}{dP}, \tag{9}$$

where dE_g^o/dP is the unstrained energy bandgap change with respect to the unit pressure.

The effect of strain on the energy band structure results in the splitting of the heavy hole and light hole band at the valence band zone center[11] (i.e., the in-plane wavevector $k_{\parallel}$ = 0), which is degenerate in the unstrained case. When tensile strain is applied between the quantum well and the barrier layers[12-14] along the superlattice growth z-direction, the strain can push the light hole levels upwards and pull the heavy hole levels downwards. We

can therefore expect that heavy hole and light hole states are inverted at specific lattice strains and quantum well thicknesses. This phenomena will in turn cause the intersubband transitions in a QWIP structure to take place from the populated light hole ground state to the upper energy band states. Since the light hole has a small effective mass (comparable to the electron effective mass), the optical absorption and photon responsivity in p-type QWIPs can be greatly enhanced, as a result of introducing strain in the quantum well. In addition to the utilization of the light hole states for their small effective masses, etc., certain heavy hole states under compressional strain may also have similar characteristics, like high mobilities, small effective masses, and long mean free paths; which in turn favorably alter the intersubband absorption and transport characteristics, as shown by Hirose, et al.[31]. This is achieved by distorting the heavy hole valence band at and near the zone center via the introduction of compressional strain.

2.2.1.3 Energy Band Calculations

To calculate the locations of the energy subbands, we can use the transfer matrix method (TMM)[13,15], based on the eight-band $\mathbf{k} \cdot \mathbf{p}$ model. This model is represented by the Luttinger-Kohn Hamiltonian[16-17], H_t, which describes the unstrained semiconductor.

$$H_t = H + V(z) \tag{10}$$

where

$$H = \begin{bmatrix} H_{11} & H_{12} & H_{13} & H_{14} \\ H_{21} & H_{22} & H_{23} & H_{24} \\ H_{31} & H_{32} & H_{33} & H_{34} \\ H_{41} & H_{42} & H_{43} & H_{44} \end{bmatrix} \tag{11}$$

with:

$$H_{11} = \frac{\gamma_1 + \gamma_2}{2}(k_x^2 + k_y^2) + \frac{\gamma_1 - \gamma_2}{2}k_z^2$$

$$H_{22} = \frac{\gamma_1 - \gamma_2}{2}(k_x^2 + K_y^2) + \frac{\gamma_1 + \gamma_2}{2}k_z^2$$

$$H_{12} = i\sqrt{3}\gamma_3(k_x - ik_y)k_z$$

$$H_{13} = \frac{\gamma_2\sqrt{3}}{2}(k_x^2 - k_y^2) - i\sqrt{3}\gamma_3 k_x k_y$$

$$H_{21} = H_{12'}^* \qquad H_{13} = H_{31'}^* \qquad H_{24} = H_{13}$$

$$H_{34} = H_{12'} \qquad H_{42}^* = H_{13'}^* \qquad H_{43} = H_{12}^*$$

$$H_{14} = H_{23} = H_{32} = H_{41} = 0$$

and V(z) is a step function where V(z) vanishes inside the well layers and equals V_o in the barrier layers. The effect of strain is included by adding the Pikus-Bir Hamiltonian[18], H_s, to the general Luttinger-Kohn Hamiltonian. As shown below, the strain Hamiltonian for the well material is a diagonal matrix.

$$H_s = \begin{bmatrix} -\Delta E_c - \Delta E_{hh} & 0 & 0 & 0 \\ 0 & -\Delta E_c + \Delta E_{hh} & 0 & 0 \\ 0 & 0 & -\Delta E_c + \Delta E_{hh} & 0 \\ 0 & 0 & 0 & \Delta E_c + \Delta E_{hh} \end{bmatrix} \tag{12}$$

Using the aforementioned techniques, we can numerically calculate the energy of the zone-center valence subband levels as a function of well width for any material system under tensile or compressional strain and also determine the change in the valence subband structures.

All of the previously described calculations are derived from the multiband effective mass $\mathbf{k} \cdot \mathbf{p}$ model for a coherently strained structure, which is based upon the perturbation approximation. In the $\mathbf{k} \cdot \mathbf{p}$ model, the interactions of S-P type coupling among conduction (C), light-hole (LH), heavy-hole (HH), and spin-orbit (SO) states combined with spin-orbit like coupling are taking into consideration to derive the band structures. This results in an 8×8 $\mathbf{k} \cdot \mathbf{p}$ Hamiltonian and momentum matrix elements. Using the pertubation approximation, a set of wave functions of $S_{1/2}$: $|1/2, \pm 1/2 >_c$; $P_{3/2}$: $|3/2, \pm 3/2 >$, $|3/2, \pm 1/2 >$; and $P_{1/2}$: $|1/2, \pm 1/2 >$ are used to represent the unperturbed and unstrained basis in the $|J, m_j >$ presentation[23]. $m_j = \pm 1/2$ represents either the electron or LH states, while $m_j = \pm 3/2$ denotes the HH or heavy particle states. A slightly simplified 6×6 $\mathbf{k} \cdot \mathbf{p}$ Hamiltonian can be used to roughly predict the P-like properties of the coherently strained layers by considering the S-like conduction band states as a pertubation, if a large enough bandgap exists, like in InGaAs and GaAs layers. The wave functions of the coherently strained superlattice at the zone center ($\mathbf{k}=0$) are given by[24]

$$|3/2, \pm 3/2 > \quad HH\,states \tag{13}$$

$$\gamma|3/2, \pm 1/2 > + \quad \beta|1/2, \pm 1/2 > \quad LH\,states \tag{14}$$

$$-\beta|3/2, \pm 1/2 > + \quad \gamma|1/2, \pm 1/2 > \quad SO\,states \tag{15}$$

where γ and β are constants which are dependent on the strain parameters. Note that the heavy-hole states, $|3/2, \pm 3/2 >$, are still decoupled from the other valence band states even under biaxial stress at the zone center, while the light-hole and spin-orbit split off states are coupled at $\mathbf{k}$=0. However, the HH, LH, and SO states are mixed[25,26] in the coherently strained superlattice at off zone center ($\mathbf{k} \neq 0$). This mixing between the states with different m_j's is due to the boundary conditions across the interface of the quantum well layers. By examining the $\mathbf{k} \cdot \mathbf{p}$ matrix, we can see that the interaction between the different m_j states is proportional to the transverse components of the wave vector, $k_{x,y}$, so that the HH states are decoupled when $k_{x,y}$=0. It is interesting to note that the $k_{x,y}$'s are conserved across the interfaces since the interface potential depends only on z, the quantum well growth direction. Thus the band mixing can be significant if the Γ-bandgap is small, e.g., with GaAs and InGaAs, and if the LH and SO bands involved in the transition have a large k_z value[25].

Since the heavy hole and light hole valence subbands are non-degenerate following the introduction of strain into the QWIP structure, a simpler method can be used to determine the energies of the subbands. By using the parabolic band approximation near the valence band zone-center, and the energy band shifts for the conduction band minimum, heavy hole subband maximum, and light hole subband maximum, we can utilize the simpler two-band Hamiltonian for electrons just by finding the effective mass of the carriers (i.e., heavy-hole effective mass and light-hole effective mass) and the barrier heights for each carrier type. Although this does not simultaneously determine the energy levels of both carriers, it does allow accurate predictions of the energy subbands. When compared to the direct calculation of the energy subbands, the two-band approximation yields accurate results when compared to the direct calculation results[13,18]. One limitation of the TMM is that this method cannot calculate the energy levels of the allowed energy subbands in the continuum states. In order to determine the transition energy from the ground state to the continuous state, we used the Kronig-Penney model to determine the locations of the allowed energy bands in the continuum states.

When a biaxial internal tension is applied to the well material, the strain pulls the LH subbands up with respect to the HH subbands for a given well thickness. While quantum confinement effects tend to push the LH subbands down with respect to the HH subbands.

As the well width is increased above a certain value, the strain effect can overcome the quantum confinement effect and therefore induce the inversion of the heavy hole and light hole subbands at the ground state. In contrast, with the application of compressional strain on the well layers, the strain forces the LH subbands down with respect to the HH subbands for a given well thickness.

2.2.1.4 The Transfer Matrix Method for the Calculation of Transmission Probability

The transfer matrix method (TMM) [33] allows the calculation of the transmission probability through a superlattice. Like any typical quantum mechanical barrier or well, the carrier conduction in each layer of the superlattice consists of the superposition of two components propagating forwards and backwards. The complete wave fuction can be expressed as

$$\psi_i = \psi_i^+ e^{+ik_i} e^{-\Delta_i} + \psi_i^- e^{-k_i} e^{+\Delta_i} \tag{16}$$

where

$$
\begin{aligned}
\Delta_1 &= \Delta_2 = 0 \\
\Delta_i &= k_i(d_2 + d_3 + \cdots + d_i \\
i &= 3, 4, \cdots, N \\
k_i &= \left[\frac{2m_i^*}{\hbar^2}(E - E_i)\right]^{1/2},
\end{aligned}
$$

where ψ_i^+ and ψ_i^- represent the magnitudes of the wave functions propagating in the forward, or $+z$ direction and the backwards, or $-z$ direction, respectively. While N is the number of periods in the superlattice, d_i is the thickness of the i-th layer in the superlattice, m_i^* is the effective mass of the particle in the i-th superlattice layer, and E_i is the potential energy of the i-th layer. Since the wave function, ψ, and it's derivative, $d\psi/dz$, are continuous at the boundaries, the wave functions then become

$$\psi_i^+ = (e^{-i\delta_i}\psi_{i+1}^+ + r_i e^{-i\delta_i}\psi_{i+1}^-)/t_i \tag{17}$$

$$\psi_i^- = (r_i e^{i\delta_i}\psi_{i+1}^+ + e^{i\delta_i}\psi_{i+1}^-)/t_i. \tag{18}$$

The recurrence relationship of the wave functions can be written in matrix form as

$$
\begin{pmatrix} \psi_i^+ \\ \psi_i^- \end{pmatrix} = \frac{1}{t_i} \begin{pmatrix} e^{-i\delta_i} & r_i e^{-i\delta_i} \\ r_i e^{i\delta_i} & e^{i\delta_i} \end{pmatrix} \begin{pmatrix} \psi_{i+1}^+ \\ \psi_{i+1}^- \end{pmatrix}, \tag{19}
$$

- 11 -

where at normal incidence

$$r_i = \frac{k_i - k_{i+1}}{k_i + k_{i+1}}, \tag{20}$$

$$t_i = \frac{2k_i}{k_i + k_{i+1}}, \tag{21}$$

and

$$\delta_i = k_i d_i. \tag{22}$$

Which gives us the following form for determining the $N + 1$-th wave functions

$$\begin{pmatrix} \psi_1^+ \\ \psi_1^- \end{pmatrix} = S_1 \begin{pmatrix} \psi_2^+ \\ \psi_2^- \end{pmatrix} = S_1 S_2 \begin{pmatrix} \psi_3^+ \\ \psi_3^- \end{pmatrix} = S_1 S_2 \cdots S_N \begin{pmatrix} \psi_{N+1}^+ \\ \psi_{N+1}^- \end{pmatrix}, \tag{23}$$

where

$$S_i = \frac{1}{t_i} \begin{pmatrix} e^{-i\delta_i} & r_i e^{-\delta_i} \\ r_i e^{i\delta_i} & e^{i\delta_i} \end{pmatrix}. \tag{24}$$

Since there is no backwards, or in the $-z$ direction, propagation in the $N + 1$-th layer, the magnitude of the wave function $\psi_{N+1}^- = 0$. Thus we can find the ψ_i^+ term of E_1^+, in the i-th layer ($i = 2, 3, 4, \cdots, N + 1$).

If we determine the quantity, ψ_i^+/ψ_1^+, as a function of E_1, then we will know the locations of the resonant peaks. The transmission probability can be expressed as

$$|T \cdot T| = \left| \frac{\psi_i^+}{\psi_1^+} \right|^2. \tag{25}$$

2.2.1.5 Determination of Intersubband Transitions and Absorption Coefficients

In addition to the energy level and energy band locations, the calculation of inter-subband and interband transitions are also of great interest. In order to determine the intersubband and interband transitions in a p-type strained layer QWIP, the usage of the 6×6 Hamiltonian which includes the previously mentioned $\mathbf{k} \cdot \mathbf{p}$ Hamiltonian[16–17,24] and the strain Hamiltonian[18]. Since the strain and the spin-orbit coupling terms do not lift the spin degeneracy, the 6×6 Hamiltonian matrix can then be factorized into two 3×3 irreducible matrices. The assumption that the Fermi distribution function is equal to one for the confined ground state and equal to zero for the excited states in equilibrium is used to simplify

the calculation without loss of accuracy. The absorption coefficient for the intersubband or interband transition between the initial ground state, i, and the final continuum state, f, is given by[27]

$$\alpha_i(\omega) = \sum_f \frac{4\pi^2 e^2}{n_r c m_o^2 \omega} \int_{BZ} \frac{2d\mathbf{k}}{(2\pi)^3} \left[(f_i - f_f) |\hat{\epsilon} \cdot \mathbf{P}_{i,f}|^2 \frac{\Gamma/2\pi}{[\Delta_{i,f}(\mathbf{k}) - \hbar\omega]^2 + (\Gamma^2/4)} \right] \quad (26)$$

where n_r is the refractive index in the quantum well, m_o is the free electron mass, $\Delta_{i,f}$ is the energy difference between the initial ground state, i, of energy $E_i(\mathbf{k})$ and the final state, f, with the corresponding energy of $E_f(\mathbf{k})$. $\hat{\epsilon}$ and ω are the unit polarization vector and the frequency of the incident IR radiation, respectively, f_i and f_f are the Fermi distribution functions of the initial and final states, and Γ is the full width of level broadening. $\Gamma \sim \hbar/\tau_{if}$, where τ_{if} is the lifetime between the initial, i, and final, f, states. $|\hat{\epsilon} \cdot \mathbf{P}_{i,f}|$ are the optical transition elements between the quantum well valence subband ground states, i, and the continuum subband states, f, in the HH, LH, and SO bands; which can be derived from the two 3×3 $\mathbf{k} \cdot \mathbf{p}$ matrix elements as shown below.

Using the following 3×3 optical matrix,

$$\frac{m_o}{\hbar} \begin{bmatrix} T_{HH} & T_{HL} & T_{HS} \\ T_{LH} & T_{LL} & T_{LS} \\ T_{SH} & T_{SL} & T_{SS} \end{bmatrix}, \quad (27)$$

the optical matrix elements, $|\hat{\epsilon} \cdot \mathbf{P}_{i,f}|$, can be obtained. These matrix elements have the same form as the $\mathbf{k} \cdot \mathbf{p}$ matrix elements except that the $k_i k_j$'s are replaced with $k_i \epsilon_j + k_j \epsilon_i$ multiplied by a constant factor of $m_o/\hbar$.[27] The T_{ij}'s are defined as follows:

$$T_{HH} = 2(A - B)\epsilon_z k_z + (2A + B)(\epsilon_x k_x + \epsilon_y k_y), \quad (28)$$

$$T_{LL} = 2(A + B)\epsilon_z k_z + (2A - B)(\epsilon_x k_x + \epsilon_y k_y), \quad (29)$$

$$T_{SS} = 2A(\epsilon_x k_x + \epsilon_y k_y + \epsilon_z k_z) \quad (30)$$

$$\begin{aligned} T_{HL} = {} & i\frac{1}{\sqrt{3}}N(\epsilon_x \cos\eta - \epsilon_y \sin\eta)k_z - i\frac{1}{3}N\epsilon_z k_\| \\ & -\sqrt{3}B(\epsilon_x k_x - \epsilon_y k_y)\cos\chi \\ & +\frac{1}{\sqrt{3}}N(\epsilon_x k_y + \epsilon_y k_x)\sin\chi, \end{aligned} \quad (31)$$

$$T_{HS} = \frac{1}{\sqrt{6}}N(\epsilon_x \cos\eta + \epsilon_y \sin\eta)k_z + \frac{1}{6}N\epsilon_z k_\|$$

- 13 -

$$+i\sqrt{6}B(\epsilon_x k_x - \epsilon_y k_y)\cos\chi$$
$$-\frac{2}{\sqrt{6}}N(\epsilon_x k_y + \epsilon_y k_x)\sin\chi, \tag{32}$$

$$T_{LS} = \left[i2\sqrt{2}B\epsilon_z + \frac{1}{\sqrt{2}}N\epsilon_x\cos(\chi-\eta) - \epsilon_y\sin(\chi-\eta)\right]k_z$$
$$-i\sqrt{2}B(\epsilon_x k_x + \epsilon_y k_y)$$
$$-\frac{1}{\sqrt{2}}N\epsilon_z k_\parallel\cos(\chi - 2\eta), \tag{33}$$

$$T_{SH} = T_{HS}^*, \tag{34}$$

$$T_{SL} = T_{LS}^*, \tag{35}$$

$$T_{LH}^* = T_{HL}^*. \tag{36}$$

Here A, B, N, χ, η are inverse mass band parameters.[27]

2.2.1.6 Photoconductive Detection Mode Operation

When IR radiation impinges on a photoconductor, the photoconductive material undergoes a physical change characterized by a change in resistance, ΔR_d. This change in resistance is due to the photo-excitation of carriers, forming mobile excess carriers in the photoconductor. The excess photogenerated carriers, Δn, can be expressed as

$$\Delta n = \frac{\eta\Delta\Phi\tau_L}{V_d} \tag{37}$$

where, η, is the quantum efficiency, $\Delta\Phi$ is the incident photon flux, τ_L is the excess carrier lifetime, and V_d is the volume of the detector. These photogenerated carriers are transported out of the detector under the influence of the applied external bias, which results in a photovoltage signal. The change in the output photovoltage, ΔV_o, due to the resistance change is given by

$$\Delta V_o = -\frac{V_a R_L \Delta R_d}{(R_L + R_d)^2}, \tag{38}$$

where R_L is the load resistance and its value is typically chosen to be about equal to R_d, the detector resistance, to match loads and to optimize the output signal.

2.2.2 P-QWIP Figures of Merit

Although our band structure and absorption calculations can be used to determine the positions of the subbands in the quantum wells, and hence determine the peak absorption

wavelength of the QWIP, many other factors must be taken into account to design a QWIP with the correct detection peak. Generally, for a high-performance QWIP, the responsivity must be high, while the noise current, and hence the dark current, must be low.

2.2.2.1 Spectral Responsivity

The responsivity, R, for a photodetector may be expressed as[19]

$$R = \frac{q\lambda\eta}{hc}G = \frac{q}{h\nu}\eta_c, \qquad (39)$$

where q is the electronic charge, λ is the wavelength of the incident photon, h is the Planck constant, c is the speed of light, η is the quantum efficiency, η_c is the collection efficiency, ν is the incident frequency, and the photoconductive gain is G. The quantum efficiency and photoconductive gain are described, respectively, by[19]

$$\eta = A\left(1 - R\right)\left[1 - exp\left(-B\alpha l_{qw}\right)\right] \qquad (40)$$

$$G = \frac{L}{t_c} \qquad (41)$$

where A is a constant that is polarization dependent, α is the absorption coefficient of the quantum well, l_{qw} is the total width of all quantum well regions, L is the mean free path of the carrier, R is the reflection coefficient, and t_c is the total width of all quantum well and barrier regions. B is a constant dependent on the number of passes IR radiation makes through the photodetector. For n-type QWIPs, A=0.5, while for p-type QWIPs A=1. The mean free path of the carrier may be expressed as[19]

$$L = \tau T_{qw}\mu_{eff}\mathcal{E}, \qquad (42)$$

where τ is the well recapture lifetime of the carrier, T_{qw} is the transmission coefficient over the quantum well, μ_{eff} is the effective mobility of the carrier, and $\mathcal{E}$ is the electric field. The effective mobility for a two-band transport model is shown to be[19]

$$\mu_{eff} = \frac{\Delta p_{lh}\mu_{lh} + \Delta p_{hh}\mu_{hh}}{\Delta p_{lh} + \Delta p_{hh}}, \qquad (43)$$

where Δp_{hh} and Δp_{lh} are the concentrations of optically induced heavy- and light- hole carriers, respectively, and μ_{hh} and μ_{lh} are the respective heavy and light hole mobilities. When only the ground state is completely occupied, either Δp_{lh} or Δp_{hh}, the optically

- 15 -

induced light holes or the optically induced heavy holes dominate, so that we may estimate μ_{eff} as the in-plane effective mass of the ground state carriers.

2.2.2.2 QWIP Collection Efficiency

A figure of merit that can be easily quantified by simple measurements is the collection efficiency, η_c. The collection efficiency describes the ease in which the energy from the incident photon flux is converted into mobile carriers which are swept out of the QWIP by the applied bias and collected; and is defined as the product of the quantum efficiency, η, and the photoconductive gain, G.

$$\eta_c = \eta G \tag{44}$$

In addition to being expressed as the mean free path over the total width of the quantum wells and barriers, G can be viewed as the ratio of the carrier transport lifetime, τ_L, to the transit time, τ_T, through the QWIP. Empirically, the photoconductive gain can be described in terms of the capture or trapping probability, p_c,[34-36]

$$G = \frac{1}{Np_c(1 + p_c)}, \tag{45}$$

and N is the number of wells. If p_c is small, then G can be approximated as, $G \simeq 1/Np_c$.

Physically, the trapping probability is defined as the ratio of the escape time from the well region to the lifetime of the excited carriers from the confined ground state. If the excited states are in resonance with the top of the barrier potential energy, then the escape time will be greatly reduced, which theoretically minimizes the trapping probability and maximizes the photoconductive gain. Therefore in all of our designs, we attempted to make the energy of the upper excited peak for the main detective peak in resonance with the top of the barrier potential energy.

If $B\alpha i_{qw} \ll 1$ and $p_c \ll 1$, an approximate expression for η_c can be written as

$$\eta_c = A(1 - R)[1 - \exp(-B\alpha l_{qw})]\frac{1 - p_c}{Np_c} \tag{46}$$

$$\approx A(1 - R)\frac{B\alpha l_{qw}}{Np_c}. \tag{47}$$

where B is a constant dependent on the number of passes the IR radiation makes through the photodetector, A is a polarization dependent variable equal to 0.5 for n-type QWIPs

and 1 for p-QWIPs, R is the reflection coefficient, l_{qw} is the total width of all quantum well regions, and α is the absorption coefficient.

2.2.2.3 Dark Current Relationship in a QWIP

Another important parameter to be considered in a QWIP design is the dark current density (J_d), which can be expressed using the Richardson-Dushman equation[14] as

$$J_d \propto T^2 m^* exp\left(\frac{-\Delta E}{kT}\right), \tag{48}$$

where m^* is the effective mass, ΔE is the difference in energy between the barrier height and the quantum confined state in the well, k is the Boltzmann constant, and T is the temperature. This type of expression assumes that the dominant source of dark current is thermionic emisson over the quantum well barrier.

In the low-field regime, the thermionic emission current is related to the density of mobile carriers, n_t and the average drift velocity, v_d, and can be expressed as[37]

$$I_{th} = eA_d v_d n_t, \tag{49}$$

where A_d is the active detector area, e is the electronic charge, and

$$v_d = \frac{\mu\varepsilon}{\left[1 + (\mu\varepsilon/v_s)^2\right]^{1/2}}, \tag{50}$$

$$n_t = \left(m^* k_b T / \pi\hbar^2 L\right) \exp\left[-\left(E_{cf} - E_F\right)/k_b T\right]. \tag{51}$$

In the above equations, μ is the mobility, ε is the electric field, v_s is the saturation velocity, E_{cf} is the cut-off energy related to the cut-off wavelength λ_c, and $m^*/\pi\hbar^2$ is the two-dimensional density of states. The Fermi energy, E_F, can be obtained from the expression of N_D:

$$N_D = \frac{m^* k_B T}{\pi\hbar^2 L} \sum_n \ln\left[1 + \exp\left(\frac{E_F - E_n}{k_b T}\right)\right] \tag{52}$$

$$\approx \frac{m^*}{\pi\hbar^2 L} \sum_n \left(E_F - E_n\right). \tag{53}$$

Equation (52) for N_D is valid when summed over the subband levels E_n below the Fermi level, and equation (53) is only valid at cryogenic temperatures.

Using the previous result in the cryogenic temperature regime, we see that the dark current due to thermionic emission is exponentially dependent on the doping concentration in the quantum well, i.e.,

$$I_{th} \propto \exp(\frac{E_F}{k_B T}) \propto \exp(\frac{N_D}{k_B T}). \tag{54}$$

Therefore, as the doping density in the quantum well increases, the dark current density due to thermionic emission also increases exponentially. In contrast to this, the intersubband absorption is directly proportional to the doping concentration. Therefore, a tradeoff between the dark current density and the intersubband absorption is required to optimize the QWIP performance. However, in the case of p-QWIPs, the Fermi level in the quantum well is pinned at or slightly above the ground state energy for highly doped quantum wells. We can increase the doping in the quantum well to increase optical absorption without increasing the dark current of the p-QWIP significantly because the thermionic emmision pinned with the Fermi level.

2.2.2.4 Noise in QWIPs

The noise in QWIP structures is mainly due to random fluctuations of thermally excited carriers. The noise is expressed as[5]

$$i_{noise} = \sqrt{4 A_d q G \Delta f J_d}, \tag{55}$$

where A_d is the detector area, and Δf is the bandwidth. Finally, a figure of merit measurement used to compare detectors is the detectivity, D^*, which is shown to be[19]

$$D^* = \sqrt{A_d \Delta f} \frac{R}{i_{noise}}. \tag{56}$$

If the dark current in a particular QWIP is lower than the 300 K background photocurrent, then the QWIP can be considered to be under background limited performance (BLIP). In a BLIP QWIP, the dominant current is due to photon noise, since all the other sources are negligible by comparison. The photon noise is calculated from the arrival statistics of the incoherent photons. The background photon noise current, i_{np}, is given by[20,21]

$$i_{np}^2 = 4 A q^2 \eta g^2 P_b B/(h\nu), \tag{57}$$

where P_b is the incident background optical power, B is the QWIP bandwidth, η is the absorption quantum efficiency, ν is the incident photon frequency, and g is the noise current

gain. The photocurrent, I_p can be approximated by

$$I_p = A(q/h\nu)\eta g P_s, \tag{58}$$

where P_s is the incident optical signal power. The constant, A, in Eqs. (46), (47), (57), and (58), is due to the polarization selectivity for n-type QWIPs versus p-type QWIPs. As previously stated, for n-type QWIPs, A = 0.5, while A = 1 for p-type QWIPs. By setting the signal-to-noise power ratio equal to unity, the background limited noise equivalent power, $(NEP)_{BLIP}$ and the detectivity, D^*_{BLIP}, for n-type QWIPs can be expressed as

$$(NEP)_{BLIP} = 2\sqrt{2h\nu BP_b/\eta}. \tag{59}$$

$$D^*_{BLIP} = \sqrt{A_d B}/(NEP)_{BLIP} = \frac{\lambda_p}{2\sqrt{2}hc}\left(\frac{\eta}{Q_b}\right)^{1/2}, \tag{60}$$

where A_d is the active area of the detector, and $Q_b = P_b/(Ah\nu)$ is the incident photon flux from the background for a given spectral bandwidth, $\Delta\nu$, and a peak wavelength, λ_p. Q_b is defined as

$$Q_b = \frac{2\pi}{c^2}\frac{\nu^2\Delta\nu}{e^{h\nu/k_bT}-1}sin^2\left(\frac{\theta}{2}\right), \tag{61}$$

where, θ, is the field of view (FOV). For a p-type QWIP, a factor of $\sqrt{2}$ is used in the denominator of Eq. (60), D^*_{BLIP}, since it can absorb both optical polarizations of the incident IR radiation.

2.3 Characterization of Strained Layer P-QWIPs

2.3.1 An InGaAs/AlGaAs on GaAs P-QWIP with compressive strain layers

A compressively strained p-QWIP based on the InGaAs/GaAs on SI GaAs was designed using the InGaAs/AlGaAs system for the quantum well/barrier structures, which was grown on the semi-insulating GaAs. With this new structure, we have demonstrated the continued viability and flexibility of the p-type compressively strained QWIP system. This structure exhibits the lowest dark current obtained for a p-type compressively strained QWIP to date, and exhibits excellent uniformity with respect to staring focal plane array applications.

The p-type compressively strained QWIP was grown on a semi-insulating GaAs substrate by molecular beam epitaxy. It consists of 20 periods of In(y $\approx$ 0.2)GaAs quantum

wells of roughly 40 $\mathring{A}$ in width p-doped to a density of approximately 2×10^{18} cm^{-3}, separated by approximately 500 $\mathring{A}$ wide undoped Al(x $\approx$ 0.15)GaAs barriers. A 0.3 μm cap layer and a 1.0 μm buffer layer of p-doped AlGaAs with a dopant density of 5×10^{18} cm^{-3} were also grown to serve as top and bottom ohmic contacts. The contact and barrier layers are roughly lattice matched to the SI GaAs substrate so that the InGaAs quantum wells are in biaxial compression with a designed lattice mismatch of nearly -1.4 %. Since the top and bottom contact layers are formed from heavily doped, large bandgap materials, a large tunneling current from the triangle potential near these ohmic contact regions may dominate the dark current of the QWIP. Therefore, rather thick undoped barrier layers of AlGaAs were grown between the contact layers and the QWIP structure to reduce this component of the dark current. A schematic diagram of this structure is shown in figure 1. The LWIR hole transition after absorption was designed to be from the heavy hole ground state (HH1) to the third heavy hole state (HH3), which is slightly below the valence band of the AlGaAs barrier. The MWIR transition is speculated to arise from the same heavy hole ground state to the (HH4) extended state. The extremely low dark current density levels most likely arise for the fact that the barrier height for thermionic emission is higher if the HH3 states were in resonance with the AlGaAs barrier.

To facilitate the characterization of this compressively strained p-QWIP, a 216 $\times$ 216 μm^2 mesa was etched onto the wafer by wet chemical etching. After patterning via a contact mask, a thin film of approximately 1200 $\mathring{A}$ of Au/Cr was deposited onto the mesa top contact and bottom buffer contact layers via e-beam deposition at a relatively slow rate for ohmic contacts. For this sample, the semi-insulating GaAs substrate was not thinned for ease of handling and simplification of the processing steps. Although this does lower the effective quantum efficiency of the device, by only letting the incident radiation have one pass through the quantum well layers. Further samples did utilize substrate thinning and a top reflective layer which indeed improved the device performance.

Figure 2 shows the dark current characteristic of the InGaAs/AlGaAs compressively strained p-QWIP. When compared with the dark current characterics of the previous compressively strained p-QWIP with a LWIR peak at $\lambda = 8.9$ μm, at similar device temperatures, the dark current for the new p-QWIP is roughly two orders of magnitude lower (see previous report). As can be clearly seen in this figure, the device is under background limited

performance (BLIP) conditions at temperatures of less than 63 K for applied biases of up to ± 3 V with BLIP temperatures of up to 70 K possible at biases of lower than approximately 1 V. When compared with the dark current characteristic of the previously studied tensile strain p-QWIP, the dark current in the compressively strained InGaAs/AlGaAs p-QWIP is still higher. Like all of the previously studied p-QWIPs, the dark current characteristic is slightly asymmetric. This can be attributed to the doping migration effect which occurs during layer growth, as previously explained[32].

Again, in this p-QWIP, the mobility of the heavy-holes are enhanced by the compressive strain in the InGaAs quantum well due to the reduction of the heavy hole effective mass by a factor of three[31]. Another effect that is attributed to the compressional strain localized in the quantum well layer is the decrease in the density of states in the well. This phenomenon causes more heavy holes to reside in higher energy states, the net effect of which is to raise the Fermi level inside the quantum well when compared to the unstrained state. This effect not only causes an increase in the number of off-center ($k \neq 0$) free heavy holes with lighter effective mass, which in turn causes a larger intersubband absorption when exposed to normal incidence IR radiation; but it also reduces the effective doping needed in the quantum well, so that the dark current is similarly reduced.

The responsivity of this p-QWIP was measured under normal incidence illumination as a function of temperature, applied bias, and incident IR radiation by using a blackbody radiation source running through an automatic PC-controlled single grating monochrometer with the appropriate filters attached. A single LWIR peak was detected at $\lambda_p = 7.4$ μm at liquid nitrogen (LN_2) temperatures (T = 77 K) and under an applied bias of 5 V, as shown in figure 3. A single MWIR peak was found at $\lambda_p = 5.5$ μm under the same conditions as previously mentioned, and is shown in figure 4. The respective responsivities for the LWIR and MWIR peaks were found to be 38 mA/W and 8 mA/W. The LWIR band is rather broad as illustrated in figure 3, with a cut-off wavelength of $\lambda_c \approx 10$ μm, which corresponds to a half-peak spectral bandwidth of $\Delta\lambda/\lambda_p = 30$ %. The asymmetrical responsivity around the spectral peak is attributed to the long-pass filter characteristic, which has a cut-on at λ = 6.7 μm. In figure 5(a), we see the peak responsivity measured as a function of bias and device temperature. As clearly seen in this figure, the responsivity is linearly proportional to the applied bias and that the variation with temperature is minimal. The MWIR peak

at $\lambda_p = 5.5$ μm has an approximate wavelength bandwidth ranging from 4 to 6.5 μm, which overlaps with the expected bandwidth of the 7.4 μm peak. For a cut-off wavelength of 6 μm, a spectral bandwidth of $\Delta\lambda/\lambda_p = 27$ % was obtained. Again, the responsivity as a function of bias was measured and a linear relation was found, as seen in figure 5(b).

Noise measurements were also performed on this p-QWIP using standard noise measurement procedures[38]. A Brookdeal 5004 low noise amplifier (LNA) which has an input referred current noise $S_{ia} \approx 4 \times 10^{-27} A^2/Hz$ was used to amplify the signal generated by this QWIP. The spectral density of the output of the LNA was measured using a HP 3561A spectrum analyzer which has a bandwidth of 100 kHz and allows data collection via computer. In order to extract the device parameters, all the measurements were carried out at temperatures higher than the device BLIP temperature of 67 K.

The noise spectral density measured at a bias of 1.0 V at 81 K was found to be 6.5 $\times$ 10^{-28} A^2/Hz. Given a device area of 216 $\times$ 216 μm^2, and a measured current responsivity of 12.5 mA/W, we calculated a detectivity, D*, of 1.06 $\times$ 10^{10} cm$\sqrt{Hz}$/W at the 7.5 μm peak wavelength. As the bias is increased, the detectivity is decreased due to the increase in dark current and the noise spectral density. The calculated D* values at 2 V and 3 V of applied bias are 6.3 $\times$ 10^9 and 3.2 $\times$ 10^9 cm$\sqrt{Hz}$/W, respectively. The noise spectral density of the the p-QWIP as a function of ambient temperature and applied reverse bias voltage is shown in figure 6. As this figure shows, at a low bias voltage, the number fluctuation noise translates into current fluctuation noise via the diffusion mechanism. As the applied bias increases, charge transport becomes drift dominant and the number fluctuation noise couples to current noise bia the hole drift mechanism; which results in a strong current dependence.[38]

The next step taken in the characterization of this p-QWIP was to create a structure that utilizes a thinned substrate layer and a reflective top contact to create a waveguide-like configuration that increases the responsivity of the QWIP without increasing the dark current and the noise of the p-QWIP, thereby raising the detectivity a proportional amount. This p-QWIP mesa structure was again created via wet chemical etching, and the same 120 $\overset{\circ}{A}$ of Cr with 1000 $\overset{\circ}{A}$ of Au was used as an ohmic contact and a reflective layer. The substrate was then polished to a thickness of 250 μm to create the waveguide-like structure while retaining quite a bit of mechanical strength. The dark current was measured at 77 K and was found to be in good agreement with that obtained from the previous device.

The responsivity was then measured using the same system, and was found to increase at least by 33%. Given that this structure has a larger mesa area (by 50%), and taking the same noise spectral density as the previous sample, we obtain a detectivity (D*) of 1.66 × 10^{10} cm$\sqrt{Hz}$/W at T = 80 K and an applied bias of 1.0 V, which gives us a roughly 50% increase in detectivity. Recent developments show that the substrate layer can be thinned even further to improve the responsivity and detectivity of the device.

2.3.2 A novel Si-doped GaAs/AlGaAs on (311) SI GaAs p-QWIP

All of the p-type QWIPs reported so far in the literature have utilized beryllium (Be) or carbon (C) for the dopant in the quantum well layers. However, both Be and C have serious shortcomings when used for high carrier concentration regions or very low resistance contact regions. The problem with carbon is that it is not very compatible with molecular beam epitaxy. Although Be can be easily used with MBE, it has the problem of a high diffusion coefficient, so that the dopant migration effect[32] occurs during layer growth in QWIPs. This effect can lead to the asymmetrical dark I-V characteristics observed in both the strained and the unstrained p-type QWIPs[4,39-40]. To cope with this phenomenon, we have successfully grown the first Si-doped p-type GaAs/AlGaAs QWIP on a SI (311) GaAs substrate. The QWIPs built from this sample do not show any of the dopant migration effect. This is due to the small diffusion coefficient of the Si impurity in the GaAs quantum well.

It has been shown that Si-doped GaAs grown by MBE exhibits a conductivity type which depends on the crystallographic orientation of the GaAs substrate and growth conditions. High concentrations of p-type doping of up to 10^{20} cm^{-3} can be achieved by doping (311) GaAs with silicon; which achieves a Hall mobility that is comparable to either Be or C doping. The GaAs/AlGaAs QWIP was grown in a Varian Modular GEN II MBE system at 550 °C, with a group V/III beam equivalent pressure (BEP) ratio of 10, which were optimized for p-doping and material quality. An acceptor concentration of 3 × 10^{18} cm^{-3} was achieved by Si-doping under the aforementioned conditions.

The Si-doped p-QWIP consists of GaAs quantum wells with a thickness of 28 $\overset{\circ}{A}$ and 300 $\overset{\circ}{A}$ wide Al$_{0.29}$Ga$_{0.79}$As barrier layers. Forty periods of the quantum well/barrier structures were grown on the (311) oriented SI GaAs substrate. The quantum wells were doped to the previously mentioned 3 × 10^{18} cm^{-3} to obtain p-type conduction in the quantum well,

while the $Al_{0.29}Ga_{0.79}As$ barriers were not doped. A 0.5 μm thick GaAs cap layer and a 1.0 μm thick GaAs buffer layer were also Si-doped to 3×10^{18} cm^{-3} to serve as ohmic contact layers. In contrast to our previous designs, a blocking barrier layer was not grown for this sample. As a result, the triangle potential formed by the heavily doped ohmic contact layers contribute to a large tunneling current which was observed in the dark I-V characteristic.

In order to test this device, a 216 $\times$ 216 μm^2 mesa was formed by means of wet chemical etching. After which a thin film of 120 $\mathring{A}$ of Cr and a 1000 $\mathring{A}$ film of Au were deposited by means of e-beam evaporation on both the cap and buffer layers to serve as ohmic contact pads. The top ohmic contact consists of a thin ring type structure around the edge of the mesa with a 50 $\times$ 50 μm^2 contact pad for electrical connection. With this contact formation, the normal incidence IR radiation is allowed to pass through the multi-quantum well layers. The technique of backside thinning to provide a waveguide-like structure and adding a reflective layer on the top of the mesa was not considered due to the mechanical brittleness of the (311) GaAs substrate; although a backside thinned structure can significantly improve the responsivity of the QWIP.

As shown in figure 7, the dark I-V characteristics of this QWIP are quite symmetrical in both the forward and reverse biased regions. This is a characteristic of uniformly doped quantum well layers, since dopants do not pile up along the growth direction of the quantum wells and therefore create a built-in electric field. Due to the lack of biaxial strain in this QWIP design, a triangular potential barrier, and the lack of a blocking barrier layer, the dark current characteristics are not as low as to be expected for a strained-layer p-QWIP. Two MWIR band peaks were found for this QWIP at 3.0 and 5.2 μm, as seen in figure 8. Although this device is based upon the 8.0 μm p-QWIP first grown by Levine, et al., the detection peak does not correspond with that predicted using his model. A possible reason for this is that during layer growth on the (311) substrate quantum wires can sometimes be formed throughout the QWIP layer structure. This phenomenon will further confine the allowed energy states in the QWIP and therefore the detective peaks will shift to the shorter wavelength bands. Another possible explanation of the detection peak wavelength shift is that the (311) substrate behaves much like the (110) substrate, which exhibits similar

responsivities in the MWIR band.

2.3.3 New compressively strained InGaAs/AlGaAs p-QWIPs for 10.1 and 9.2 μm detection

Although the LWIR band ranges from 8 μm to above 14 μm, the main wavelength for usable detectors can be found at or near 10 μm. Thus, there is a need to develop and characterize p-QWIPs with peak detectivity and responsivities at or near 10 μm. After analyzing the data obtained form the 7.4 μm compressively strained-layer p-QWIP, we have determined that the proper band offset in the InGaAs/AlGaAs system is closer to a 60/40 split with the conduction band offset being 60% of the difference in bandgap energies. Using this information, we have designed two new Be-doped p-QWIPs with peak detective wavelengths at 9.2 and 10.1 μm. Both of these designs utilize the ground state heavy hole (HH1) to third bound state heavy hole (HH3) transition for LWIR detection. The HH3 state was designed to be in resonance with the edge of the barrier valence band edge for lowered dark current and high responsivity. With the HH3 in resonance with the barrier valence band edge, it was expected that the responsivity curve could be much broader than that obtained previously with the 7.4 μm design which utilized a bound-to-bound state transition for detection in the LWIR band.

Similar to the previous p-QWIPs the 200 $\times$ 300 μm^2 mesas for these two QWIPs were created by wet chemical etching. Afterwards, a 120 $\mathring{A}$ thick layer of Cr was deposited, along with a 1000 $\mathring{A}$ thick layer of Au, to create the ohmic contacts and in this case a top reflective layer. The (100) SI GaAs substrate was then mechanically lapped to a thickness of 150 μm to create the waveguide-like structure which the incident IR radiation passes through. It was found that this substrate thickness was more efficient than the 250 μm structure and that it still had the mechanical strength to stand up to the ultrasonic bonding process which electrically connected the QWIPs.

As seen in figures 9 and 10, the dark current characteristics for each of these p-QWIPs is rather high. If we compare the dark current at a certain temperature for each QWIP, we see that there is a three times increase in dark current when comparing the 10.1 μm p-QWIP with the 9.2 μm one. This agrees with the thermionic emission theory since the difference in energy of these two levels is about 11 meV. Figure 11 shows the current responsivity of the 10.1 μm p-QWIP. From this graph, we obtain a maximum responsivity, R_A, of 17 mA/W

under an applied bias of -1.0 V at 55 K. Using the lock-in amplifier to obtain a rough estimate of the spectral noise density, $S_n \approx 1.6 \times 10^{-25} A^2/\sqrt{Hz}$. When combined with the mesa area, we calculate a detectivity, D*, at 10.1 μm of 1.04 $\times$ 10^9 cm$\sqrt{Hz}$/W. Further studies on the noise characteristics of this 10.1 μm p-QWIP and the 9.2 μm p-QWIP are currently being pursued. It is interesting to note the relative wideness of the responsivity curve especially compared to the two-color 7.4 μm peak curve. The FWHM spectral bandwidth of this detector was found to be $\Delta\lambda/\lambda = 40\%$. Figure 12 shows the current responsivity of the 9.2 μm peak p-QWIP. Note the extreme broadness of this responsivity curve with a peak at 9.2 μm which corresponds to a responsivity of 28 mA/W. The FWHM spectral bandwidth of this device is estimated at $\Delta\lambda/\lambda = 54\%$ since the shorter wavelength cut-off was abruptly terminated by the long-pass filter which has a cut-on at 6.7 μm. Again, using the lock-in amplifier to obtain an estimate of the noise spectral density of the device, $S_n \approx 6.4 \times 10^{-25} A^2/\sqrt{Hz}$. Using this information and the device area with the measured responsivity, we determine a detectivity at 9.2 μm and T = 45 K with an applied bias of -2.5 V of 2.7 $\times$ 10^9 cm$\sqrt{Hz}$/W. Although the the forward bias responsivity is slightly lower than that measured for the reverse bias case, e.g. 22 mA/W at T=45 K and V=3.0 V we can expect a higher detectivity due to the lower dark current and the lower corresponding spectral noise density. Further modifications on this design are in progress in an attempt to lower the dark current density, and the corresponding noise spectral density, in addition to narrowing the responsivity curve. Additionally, further studies into a MWIR peak for both of these p-QWIPs and further characterization of these p-QWIPs at higher temperatures are currently being pursued.

2.4 Conclusion and Remarks

Over the last half-year period, we have achieved a better understanding in regards to the design and characterization of P-QWIPs. We previously demonstrated a novel strained-layer design that utilizes biaxial tension on an InP substrate with ultra-low dark current, high detectivity, high responsivity, and BLIP operation. We have also demonstrated a reliable, novel compressively strained-layer designs on a GaAs substrate with detective peaks at 7.4, 8.4, 8.9, 9.2, and 10.1 μm in the LWIR band and 5.5 μm in the MWIR band with high detectivity, high responsivity, and high gain. We have demonstrated detectivities of 4.0 $\times$

10^9, 1.66×10^{10}, 2.7×10^9, and 1.04×10^9 cm$\sqrt{Hz}$/W with the 8.9, 7.4, 9.2, 10.1 μm peak wavelength p-QWIPs. In addition, we have initially explored the possibility of using Si as an acceptor dopant in InGaAs/GaAs/AlGaAs on (311) SI GaAs substrates to eliminate the dopant migration effect and therefore create a highly symmetric dark current characteristic.

References

1. B. F. Levine, R. J. Malik, J. Walker, K. K. Choi, C. G. Bethea, D. A. Kleinman, and J. M. Vandenberg, Appl. Phys. Lett. **50**, 273 (1987).

2. L. S. Yu, S. S. Li, Appl. Phys. Lett. **59**, 1332 (1991).

3. G. Hasnain, B. F. Levine, C. G. Bethea, R. A. Logan, J. Walker, and R. J. Malik, Appl. Phys. Lett. **54**, 2515 (1989).

4. J. Y. Andersson and L. Lundqvist, J. Appl. Phys. **71**, 3600 (1992).

5. B. F. Levine, S. D. Gunapala. J. M. Kuo, S. S. Pei, and S. Hui, Appl. Phys. Lett. **59**, 1864 (1991).

6. J. Katz, Y. Zhang, and W. I . Wang, Electron. Lett. **28**, 932 (1992).

7. W. S. Hobson, A. Zussman, B. F. Levine, and J. deJong, J. Appl. Phys. **71**, 3642 (1992).

8. J. W. Matthews and A. E. Blakeslee, J. Cryst. Growth **32**, 265 (1976).

9. Landolt-B(o)rnstein, "Numerical Data and Functional Relationships in Science and Technology", O. Madelung, ed., Group III, **17a, 22a**, Springer-Verlag, Berlin (1986).

10. G. Ji, D. Huang, U. K. Reddy, T. S. Henderson, R. Houre, and H. Morkoç, J. Appl. Phys. **62**, 3366 (1987).

11. T. P. Pearsall, Semiconductors and Semimetals, **32**, 55 (1990).

12. H. Asai, and Y. Kawamura, Appl. Phys. Lett. **56**, 746 (1990).

13. H. Xie, J. Katz, and W. I. Wang, Appl. Phys. Lett. **59**, 3601 (1991).

14. R. T. Kuroda and E. Garmire, Infrared Phys. **34**, 153 (1993).

15. L. R. Ram-Mohan, K. H. Yoo, and R. L. Aggarwal, Phys. Rev B **38**, 6151 (1988).

16. J. M. Luttinger and W. Kohn, Phys. Rev. **97**, 869 (1956).

17. J. M. Luttinger, Phys. Rev. **102**, 1030 (1956).

18. G. L. Bir and G. E. Pikus, "Symmetry and Strain-Induced effects in Semiconductors", Wiley, New York (1974).

19. E. L. Derniak and D. G. Crowe, Optical Radiation Detectors, Wiley, New York (1984).

20. B. F. Levine, C. G. Bethea, G. Hasnain, J. Walker, and R. J. Malik, Appl. Phys. Lett. **53**, 296 (1988).

21. D. A. Scribner, M. R. Kruer, and J. M. Killiany, Proc. of the IEEE **79**, 66, (1991).

22. R. Hull, J. C. Bean, F. Cerdeira, A. T. Fiory, and J. M. Gibson, Appl. Phys. Lett. **48**, 56 (1986).

23. E. O. Kane, "Semiconductors and Semimetals", eds. R. K. Willardson and A. C. Bear, **1**, 75 (1966).

24. F. H. Pollack, "Semiconductors and Semimetals", ed. T. P. Pearsall, **32**, 17 (1990).

25. Y. C. Chang and R. B. James, Phys Rev. **B-39**, 672 (1989).

26. P. Man and D. S. Pan, Appl. Phys. Lett. **61**, 2799 (1992).

27. S. K. Chun, D. S. Pan, and K. L. Wang, Phys. Rev. **B-47**, 15638 (1993).

28. B. F. Levine, J. Appl. Phys. **74**, R1 (1993).

29. J. W. Matthews and A. E. Blakeslee, J. Cryst. Growth **27**, 118 (1974).

30. J. W. Matthews and A. E. Blakeslee, J. Cryst. Growth **29**, 273 (1975).

31. K. Hirose, T. Mizutani, and K. Nishi, J. Cryst. Growth **81**, 130 (1987).

32. H. C. Liu, Z. R. Wasilewski, and M. Buchanan, Appl. Phys. Lett. **63**, 761 (1993).

33. A. K. Ghatak, K. Thyagarajan, and M. R. Shenoy, IEEE J. Quantum Electron. **24**, 1524 (1988).

34. H. C. Liu, Appl. Phys. Lett. **60**, 1507 (1992).

35. H. C. Liu, Appl. Phys. Lett. **61**, 2703 (1992).

36. W. A. Beck, Appl. Phys. Lett. **63**, 3589 (1993).

37. S. D. Gunapala, B. F. Levine, and K. West, J. Appl. Phys. **69**, 6517 (1991).

38. D. C. Wang, G. Bosman, Y. H. Wang, and S. S. Li, J. Appl. Phys. **77**, 1107 (1995).

39. Y. H. Wang, S. S. Li, J. Chu, and Pin Ho, Appl. Phys. Letts., **64**,727 (1994).

40. Y. H. Wang, J. C. Chiang, and S. S. Li, and Pin Ho, J. Appl. Phys. **76**, 2538 (1994).

Device (strain)	λ_p (μm)	Responsivity (mA/W)	Dark Current Density (A/cm^2) @ 77 K, 1 V
InGaAs/InAlAs (tensile)	8.1	18	5×10^{-8}
InGaAs/GaAs (compressive)	8.9, 8.4, 5.5	45	2.5×10^{-2}
InGaAs/AlGaAs (compressive)	7.4, 5.5	38	1.1×10^{-4}
InGaAs/AlGaAs (compressive)	9.2	28	1.6×10^{-2}
InGaAs/AlGaAs (compressive)	10.1	17	5×10^{-2}

Table 1. Comparison of the strained layer p-QWIPs studied so far.
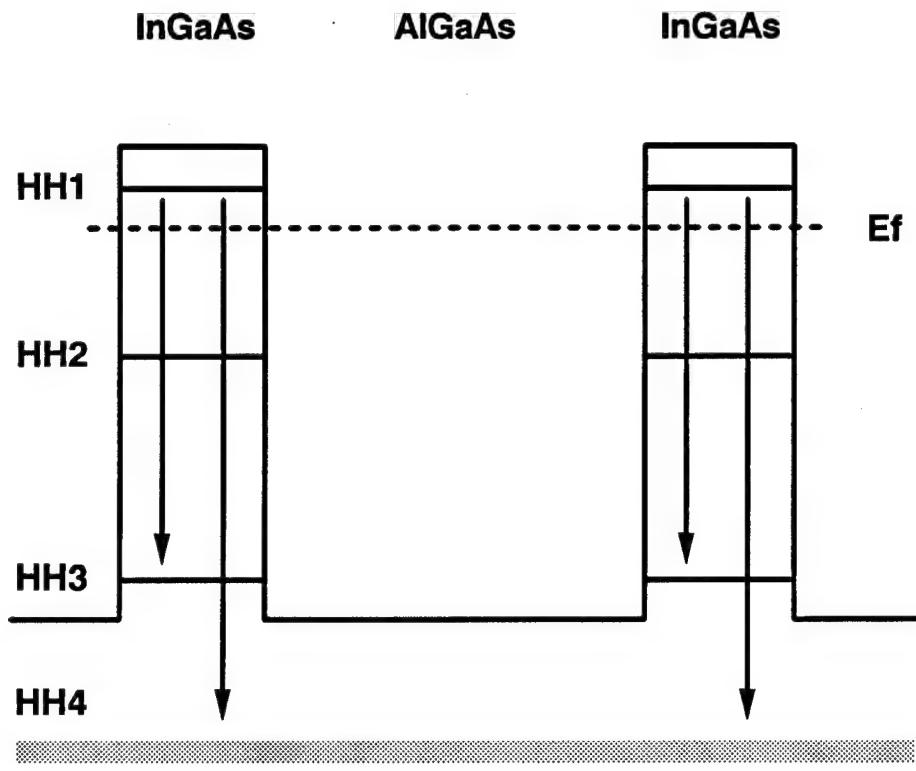
Figure 1: The schematic diagram for the two-color two-band compressively strained InGaAs/AlGaAs p-QWIP.
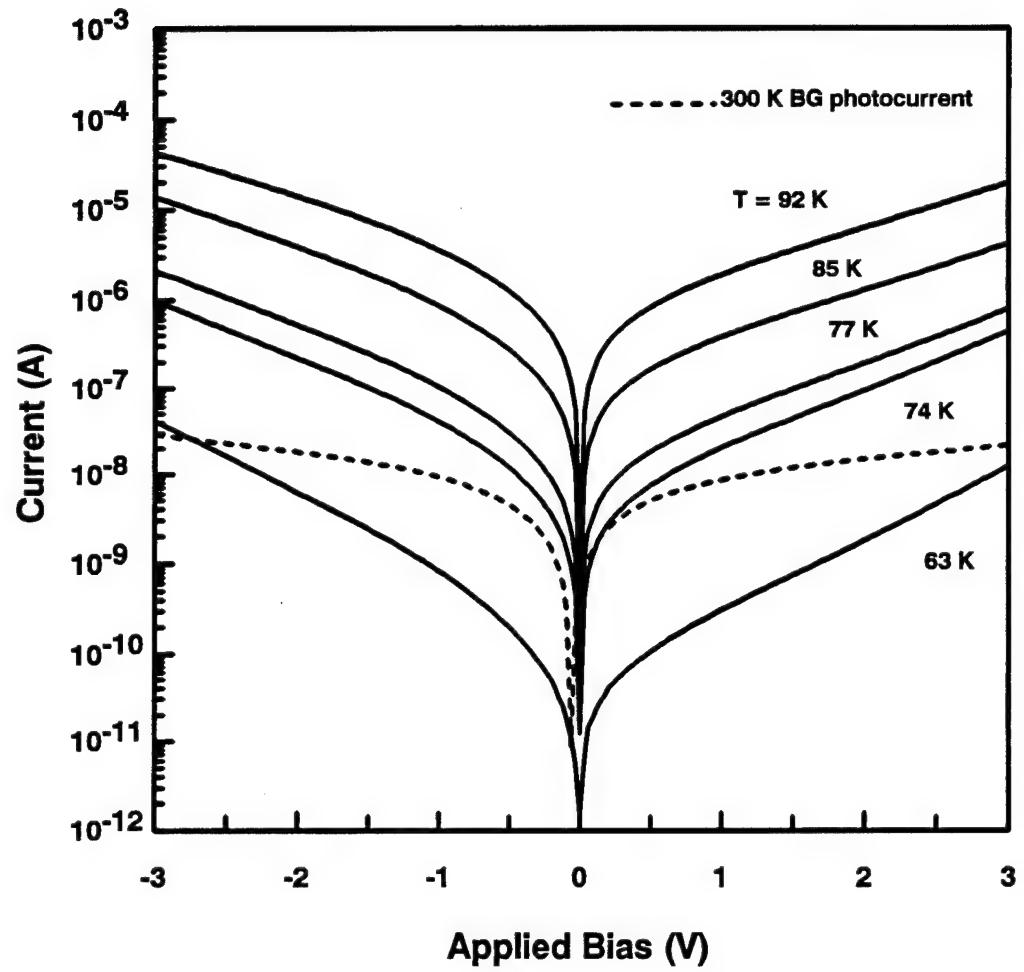
Figure 2: Dark current characteristic of the InGaAs/AlGaAs CSL p-QWIP.
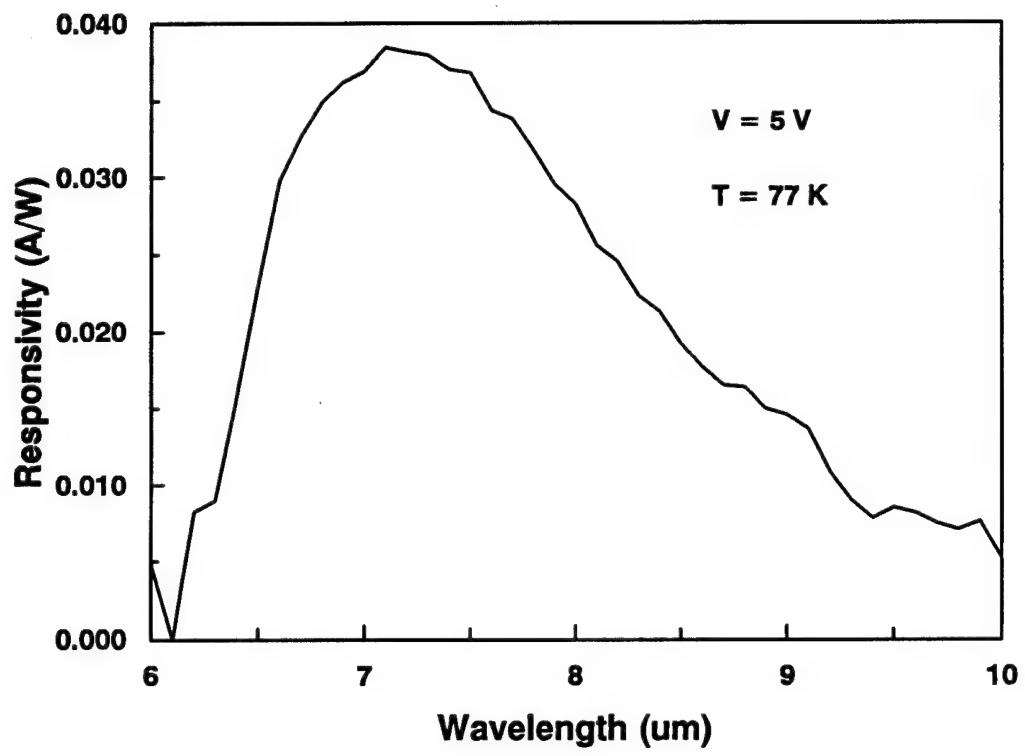
Figure 3: LWIR responsivity of the InGaAs/AlGaAs CSL p-QWIP at 77 K and +5.0 V bias.
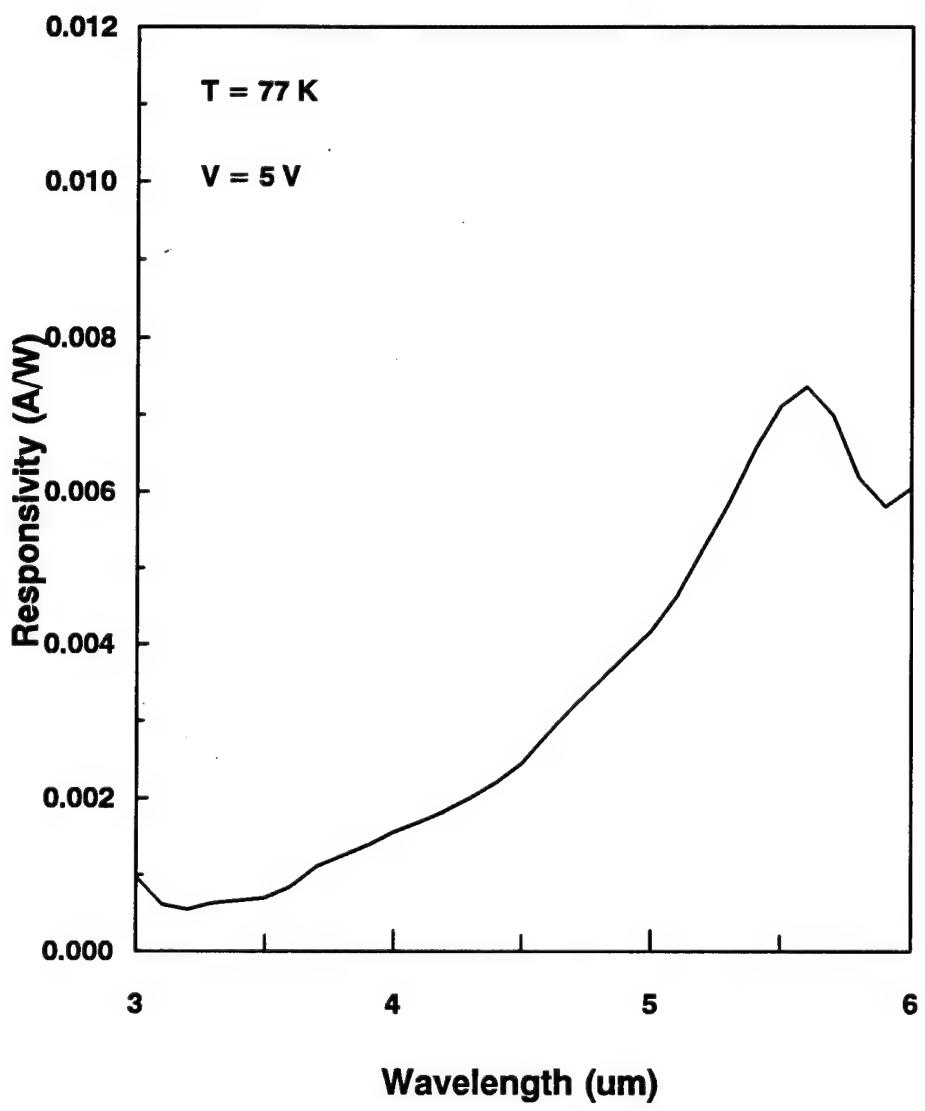
Figure 4: MWIR responsivity of the InGaAs/AlGaAs CSL p-QWIP at 77 K and +5.0 V bias.
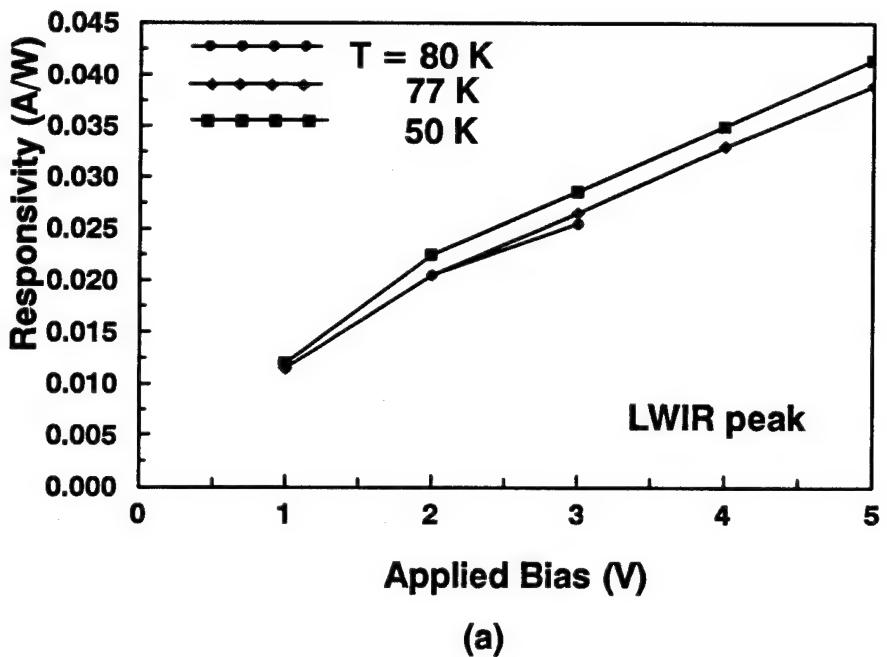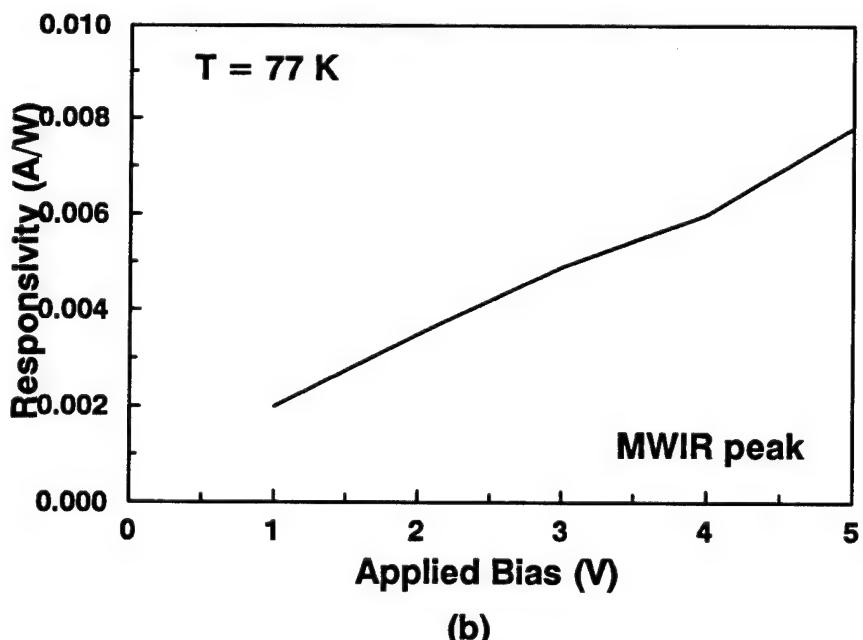
Figure 5: (a) LWIR responsivity at $\lambda_p = 7.4$ μm and (b) MWIR responsivity at $\lambda_p = 5.5$ μm as a function of applied bias and temperature.
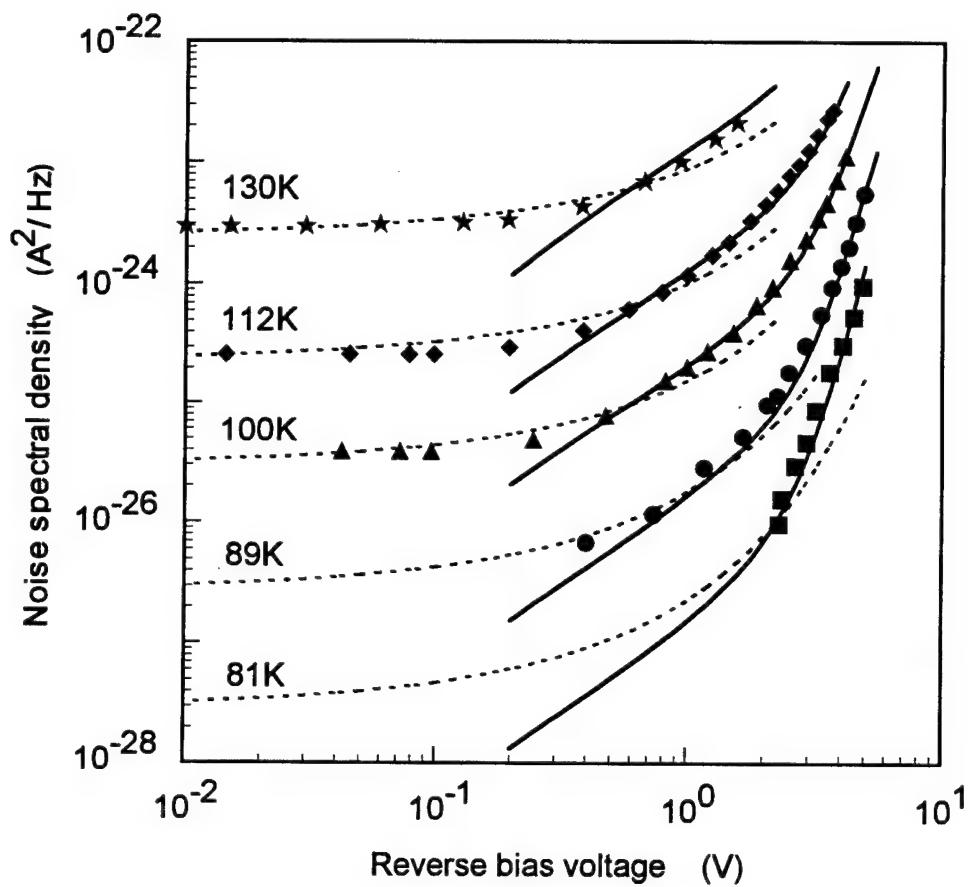
Figure 6: Experimental and theoretical current noise spectral density versus reverse bias voltage for various temperatures.
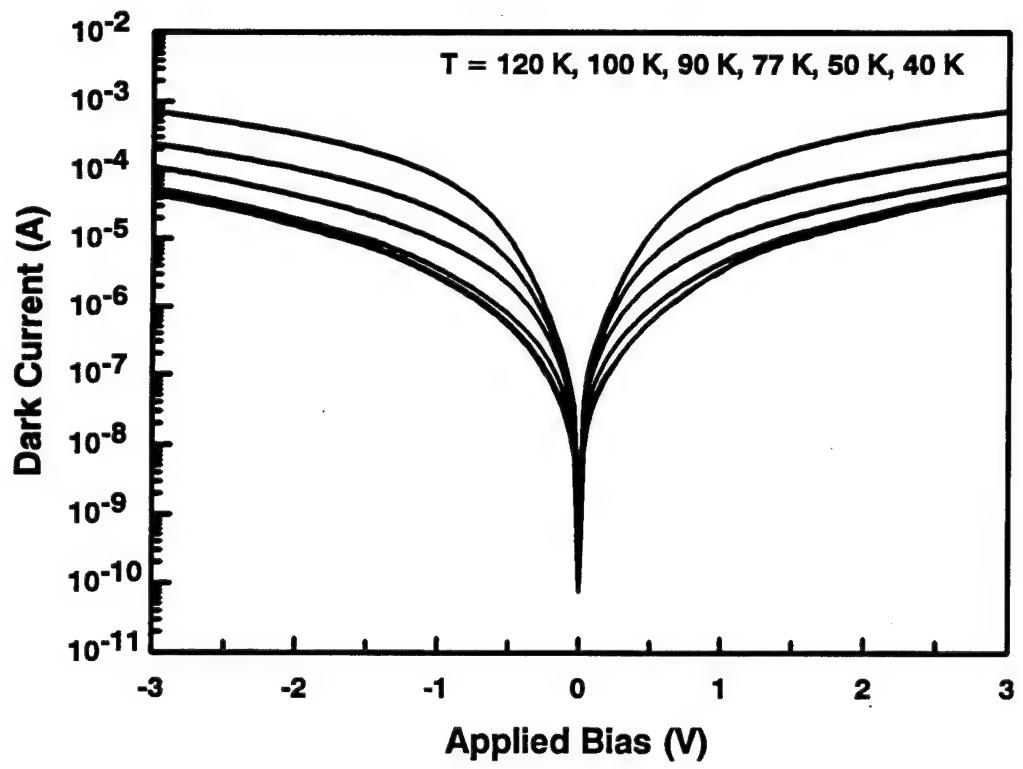
Figure 7: Dark current characteristic for the Si-doped unstrained GaAs/AlGaAs p-QWIP.
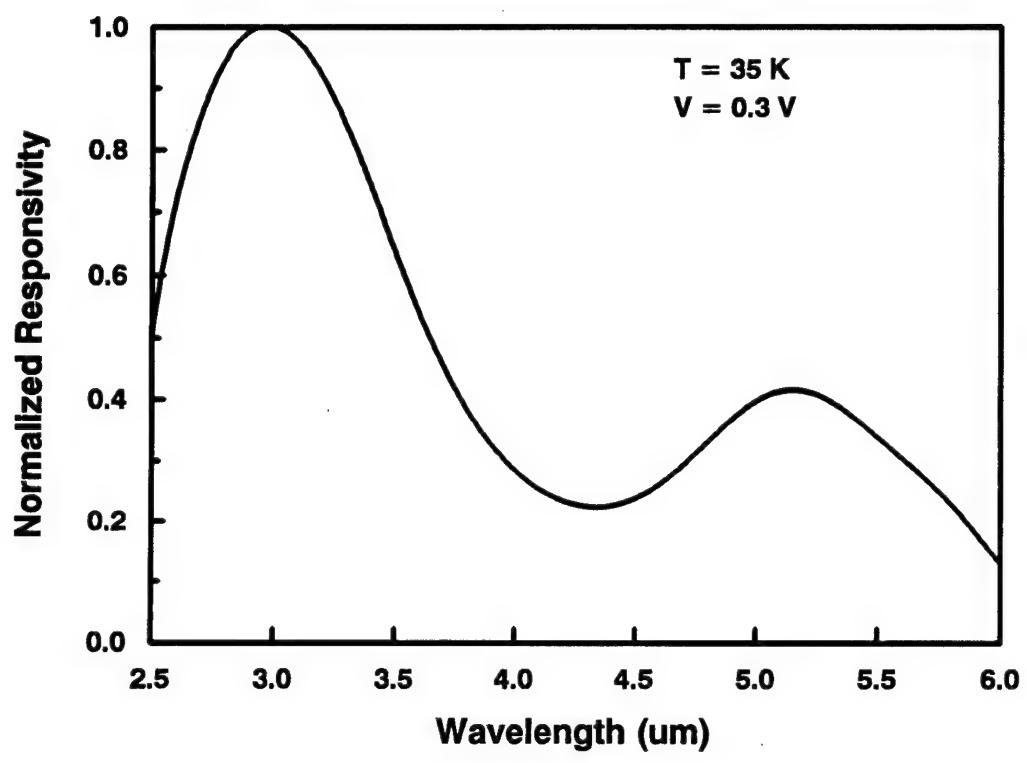
Figure 8: Normalized responsivity for the Si-doped p-QWIP.
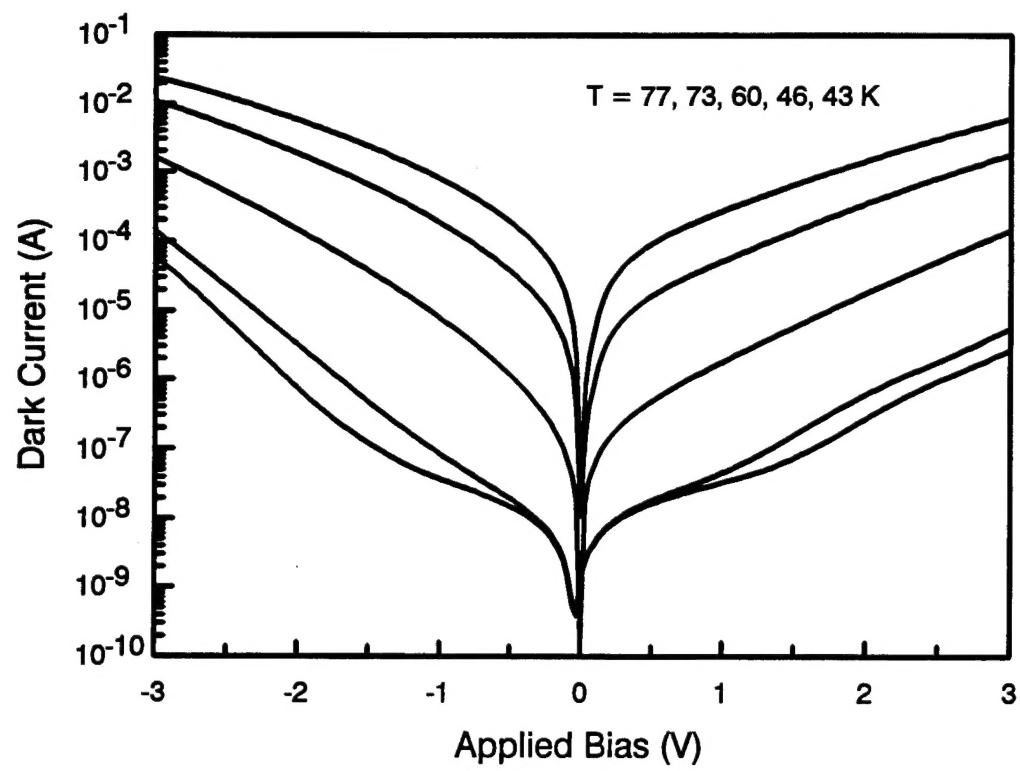
Figure 9: Dark current characteristic for the CSL InGaAs/AlGaAs p-QWIP with a detective peak at $\lambda_p = 10.1$ μm.
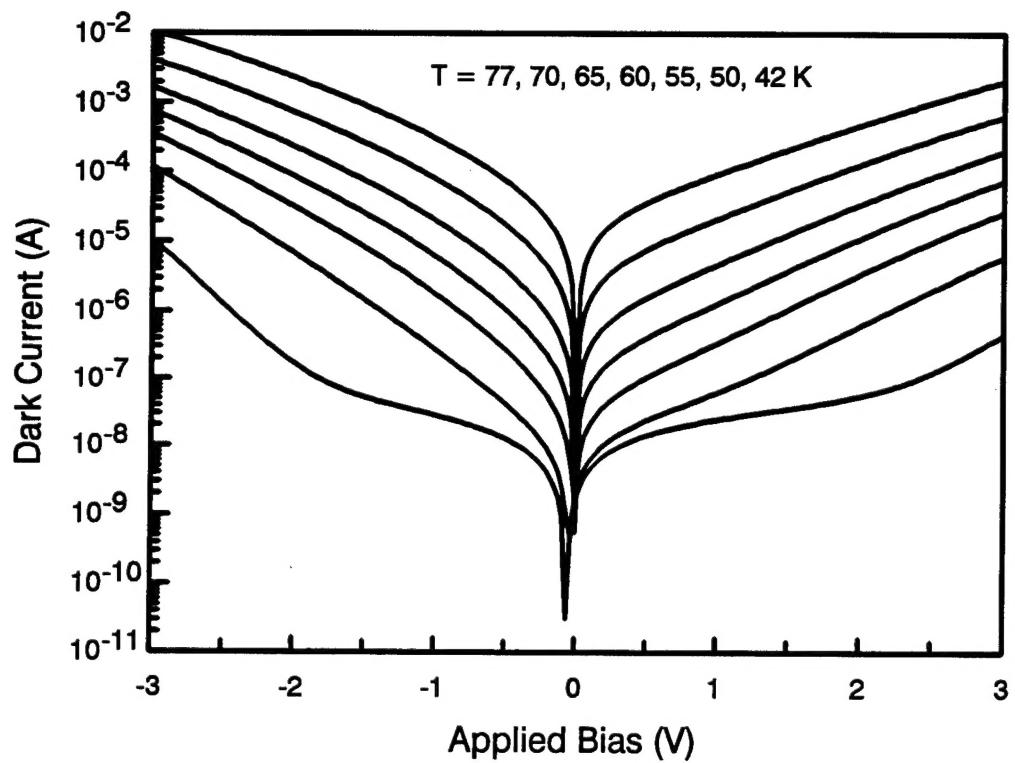
Figure 10: Dark current characteristic for the CSL InGaAs/AlGaAs p-QWIP with a detective peak at $\lambda_p = 9.2$ μm.
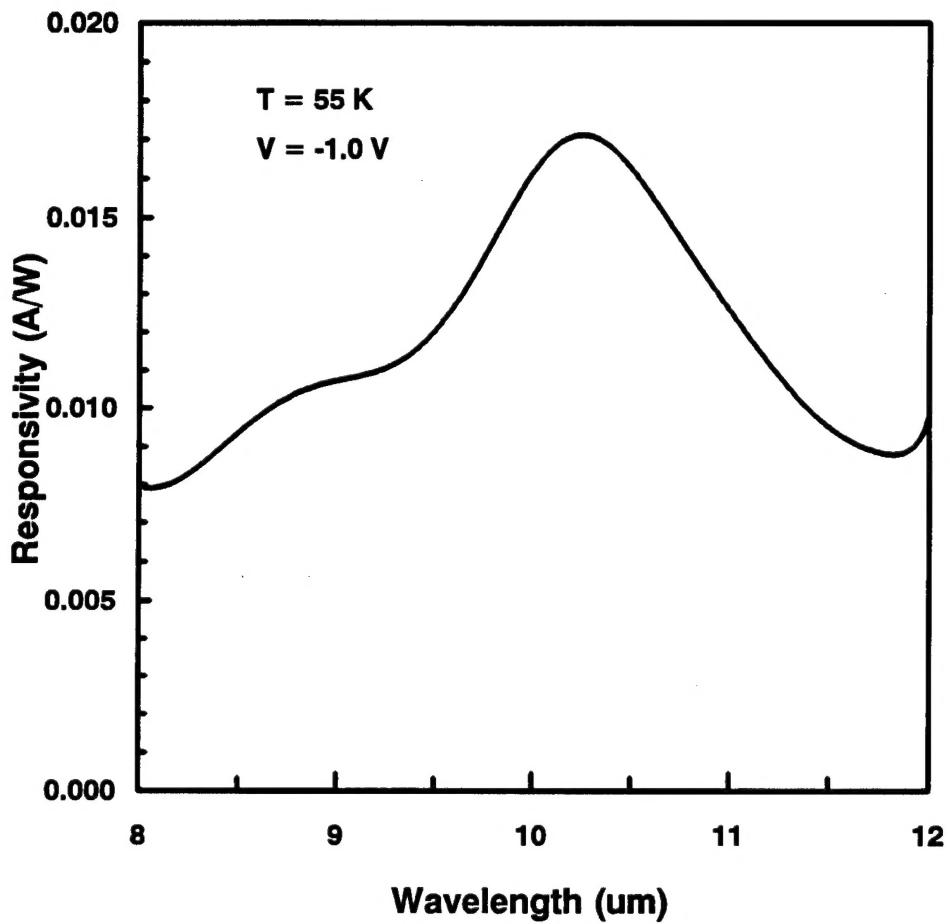
Figure 11: Measured LWIR responsivity of the $\lambda_p = 10.1$ μm CSL p-QWIP at 55 K and -1.0 V bias. Estimated D* $= 1.04 \times 10^9$ Jones.
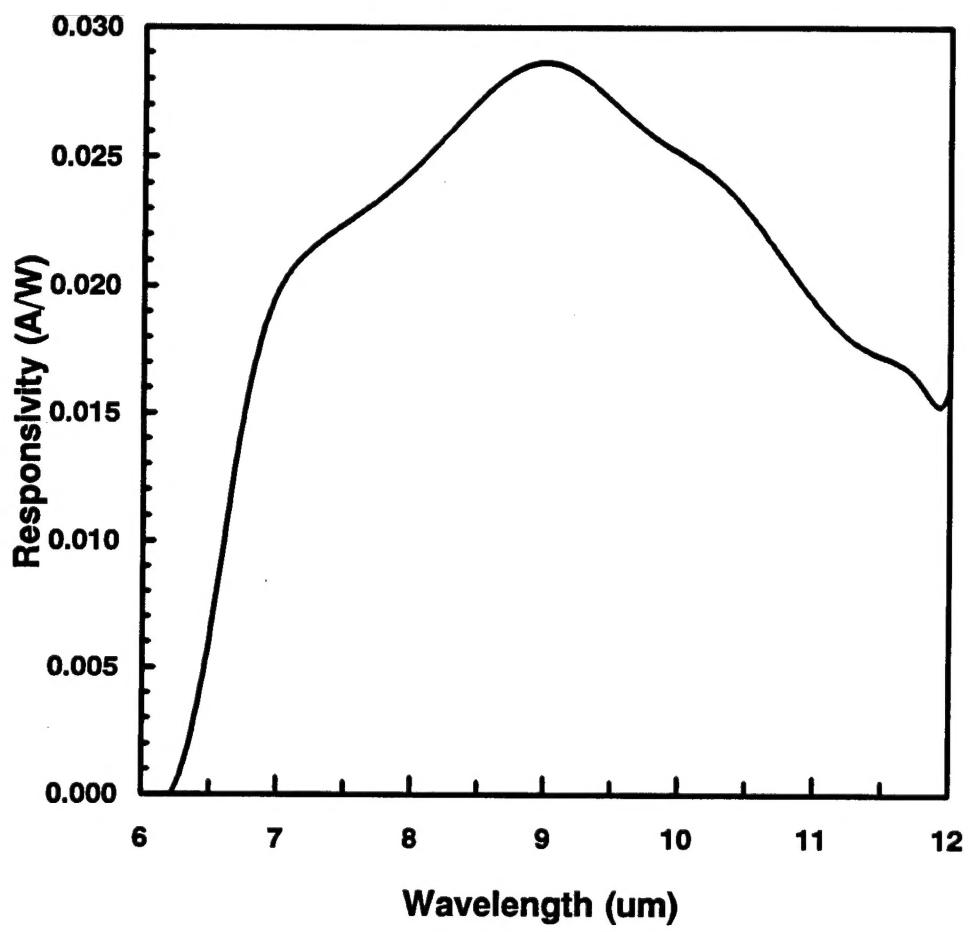
Figure 12: Measured LWIR responsivity of the $\lambda_p = 9.2$ μm CSL p-QWIP at 45 K and -2.5 V bias. Estimated $D^* = 2.7 \times 10^9$ Jones.